JGR Earth Surface

RESEARCH ARTICLE
10.1029/2021JF006435

Preservation and Completeness of Fluvial Meandering Deposits Influenced by Channel Motions and Overbank Sedimentation

Jean-Louis Grimaud[1], Fabien Ors[1], Martin Lemay[1,2], Isabelle Cojan[1], and Jacques Rivoirard[1]

[1]MINES ParisTech, PSL University, Centre de Géosciences, Fontainebleau Cedex, France, [2]Modis, Technopole Hélioparc, Pau-Pyrénées, Bâtiment Newton, Pau, France

Key Points:

- Fluvial meandering simulations used to track topographic and facies changes to resolve the influence of stasis and reworking on completeness
- Timescale for visiting the floodplain corresponds to the transition from anti-persistent to persistent depositional regimes
- New simple formulation to assess average completeness

Supporting Information:

Supporting Information may be found in the online version of this article.

Correspondence to:

J.-L. Grimaud,
jean-louis.grimaud@mines-paristech.fr

Citation:

Grimaud, J.-L., Ors, F., Lemay, M., Cojan, I., & Rivoirard, J. (2022). Preservation and completeness of fluvial meandering deposits influenced by channel motions and overbank sedimentation. *Journal of Geophysical Research: Earth Surface*, *127*, e2021JF006435. https://doi.org/10.1029/2021JF006435

Received 17 SEP 2021
Accepted 26 APR 2022

Author Contributions:

Conceptualization: Jean-Louis Grimaud, Fabien Ors, Isabelle Cojan
Data curation: Jean-Louis Grimaud
Formal analysis: Jean-Louis Grimaud, Jacques Rivoirard
Investigation: Martin Lemay, Isabelle Cojan, Jacques Rivoirard
Methodology: Jean-Louis Grimaud, Fabien Ors, Martin Lemay, Jacques Rivoirard
Software: Jean-Louis Grimaud, Fabien Ors, Martin Lemay
Supervision: Jean-Louis Grimaud
Validation: Jean-Louis Grimaud, Fabien Ors, Isabelle Cojan, Jacques Rivoirard
Writing – original draft: Jean-Louis Grimaud
Writing – review & editing: Fabien Ors, Martin Lemay, Isabelle Cojan, Jacques Rivoirard

Abstract Assessing the contribution of geomorphic processes to the (non-)preservation of sedimentary deposits is necessary to account for potential bias in measured accumulation rates in the stratigraphic record. In this study, a series of numerical simulations of fluvial meandering successions is performed using FLUMY, a model of channel motions and sedimentary facies deposition. We develop tools to measure non-deposition (stasis S) and reworking (R) of previously deposited sediment between iterations, which are both generators of hiatuses in the sedimentary record. We then compare S and R with measurements of accumulation rates and completeness (C). Results show that combining measurements of both topographic and facies changes allows for a better record of surface evolution than measuring topographies only. Accumulation rate dependence on measurement time span allows distinguishing between two regimes. The first one (anti-persistent) is characteristic of channel avulsion and compensational stacking until the whole domain is visited by overbank deposition, corresponding to the visitation timescale T_v. In the second regime (persistent), reworking by channel migration is the remaining active process until the whole system has aggraded one channel depth, corresponding to the compensation timescale T_c. Based on these results, we propose a new simple formulation based on stasis and reworking to estimate average completeness.

Plain Language Summary Sedimentary rocks contain a record of Earth's past environments and evolution, which has a lot of missing information. This is due to sedimentary processes dynamics. In the case of fluvial systems, deposition is limited to the area near rivers while the remaining landscape is "inactive." With time, rivers move to other locations, which accumulate sediment, whereas abandoned area do not anymore. In addition, river channels are erosive and can remove previously accumulated sediment: part of the record is then lost. The greater the recording time, the more information is missing. This study explores the factors that have an influence on time preservation in rocks in the case of meandering rivers deposits. To that purpose, we use a numerical model of a river-swept alluvial plain. We track changes of the depositional record with time using several indicators: the sediment deposition rates, the fraction of inactive surface and the fraction of erased record. Compared to previous studies, we measure changes of the sediment record between iterations in addition to measures of topographic change, which gives better results to assess time preservation. This leads us to propose a new formulation for estimating the average time preservation in sedimentary records.

1. Introduction

Preserved sedimentary accumulations record Earth's past geography, life and climate, as well as mass redistribution by surface processes. The probability of having continuous deposition and subsequent preservation in one location however is low (Ager, 1973). The question is then how meaningful is a measure of accumulation rate and how does it compare with other measured rates (Tipper, 1998; S. Trampush et al., 2017). Global compilations demonstrate that, in any depositional environment, sediment accumulation rates span orders of magnitude, and decrease when increasing the time-interval (time span) at which they are measured (Sadler, 1981). This "Sadler effect" is explained by the increasing incorporation with time of hiatuses in 1D sections (Plotnick, 1986) (Figure 1), a bias that can be lessened using 2D vertical sections and, in some cases, overcome when using large scale 3D data sets (Sadler & Jerolmack, 2015; Wheeler, 1958).

At the scale of outcrops, particularly in fluvial sections, hiatuses are nevertheless dominant: the stratigraphic record is incomplete. Current methods for assessing completeness based on strata geometry analysis are in their early stages (Holbrook & Miall, 2020; Tipper, 1998; S. Trampush et al., 2017; S. M. Trampush & Hajek, 2017)

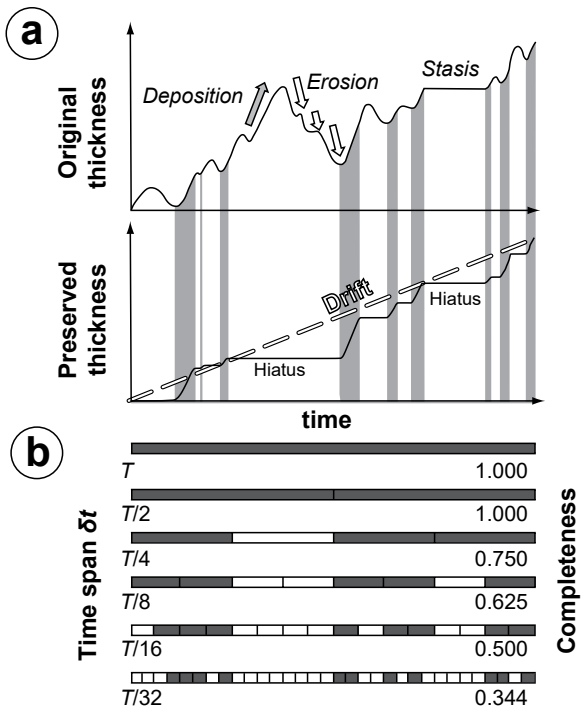

Figure 1. (a) Theoretical 1D evolution of the elevation at a 2D location in a depositional system. Erosion events induce differences between original thickness (top) and preserved thickness (bottom). Gray areas correspond to hiatus, which can arise from two processes: stasis (non-deposition) or erosion. (b) Measure of completeness associated with the evolution in panel (a) based on the preserved sediment thickness at different time span. Dark gray areas correspond to intervals that have left a record. Completeness is the ratio of the sum of intervals that have left a record to the total number of intervals (after Sadler, 1981).

and will improve with knowledge on how morphodynamics impact stratigraphic completeness (Straub et al., 2020). The sources of hiatuses themselves are characteristic of geologic processes, that is, from erosion/transport to large-scale climatic and tectonic forcing (e.g., Holbrook & Miall, 2020; Paola et al., 2018; Reesink et al., 2015). Knowledge on hiatus formation is thus potentially additional information for reconstructing paleo-environments and sediment transfers (Figure 2a). Of particular importance are (a) sediment reworking (i.e., cannibalism), which is among the storage and release processes that buffer sediment transfers along large rivers (e.g., Jerolmack & Paola, 2010; Métivier & Gaudemer, 1999), and (b) stasis, which consists in pauses of the record in a depositional sense (Miall, 2015; Tipper, 2015) but that can be recorded for instance in alluvial systems with the development of paleosols (e.g., Abels et al., 2013; Grimaud et al., 2020; Retallack, 1984).

Theory on completeness has improved in the past decades through the development of 1D mathematical models and, more recently, the study of completeness on experimental fan deltas. Using numerical simulations, the dependence of accumulation rates on measurement interval (with power-law attributes) was investigated in relation with the distribution of hiatuses (Ganti et al., 2011; Schumer et al., 2011). Studies also focused on the saturation timescale, where the Sadler effect theoretically fades out (Jerolmack & Sadler, 2007). It was showed theoretically (Schumer & Jerolmack, 2009; Schumer et al., 2011) and experimentally (Straub & Esposito, 2013) that this timescale equaled the compensational timescale T_c, that is, the time necessary for sedimentation to fill the topographic roughness -usually the maximum channel depth.

Much of the many recent advances on completeness were thus theoretical and based on topographic analysis. In fluvial systems, a missing part is the irremediable replacement of facies by another (~facies replacement) that is not captured when using topographic clipping (i.e., difference between two topographies). It is exemplified by the replacement of overbank deposits by point bar as a fluvial channel migrates laterally (Figure 2b). In this study, we use FLUMY, a model that generates a fluvial meandering channel and associated deposits (point bars and overbank sedimentation), to track topographic and depositional changes and calculate completeness. Accumulation rates measured at different time intervals in seven simulations, allow distinguishing between an anti-persistent and a persistent regime (see next section for definitions). We discuss in turn the specificities of these two regimes and how their characteristics can help quantify the mean completeness of fluvial deposits.

2. Background

2.1. Measured Accumulation Rates and Completeness of a Fluvial Meandering Section

Accumulation rates available in syntheses mostly consist of positive rates measured on 1D sections (~boreholes) using field observation, survey reoccupation or absolute radiometric dating (Sadler, 1981). They are not equivalent to measurements of accumulation over 2D domains (~maps), which also average area without deposition and are thus less biased (Sadler & Jerolmack, 2015). The vertical rates can nevertheless be recovered using the average of accumulation in a 2D domain D over the depositional area only (i.e., excluding inactivity or stasis S) (Figure 2a). For a given time span δt that divides a total duration T, the average 1D rate of accumulation is then:

$$A_{\delta t} = \frac{\sum_{j=1}^{N} (V_{\delta t j})}{T D (1 - S_{\delta t})} \quad (1)$$

where $V_{\delta t}$ is a measure of sediment volume accumulated during one interval, $N = T/\delta t$ the number of intervals, and $S_{\delta t}$ the average stasis fraction in the domain (see Supporting Information S1). There are several ways to

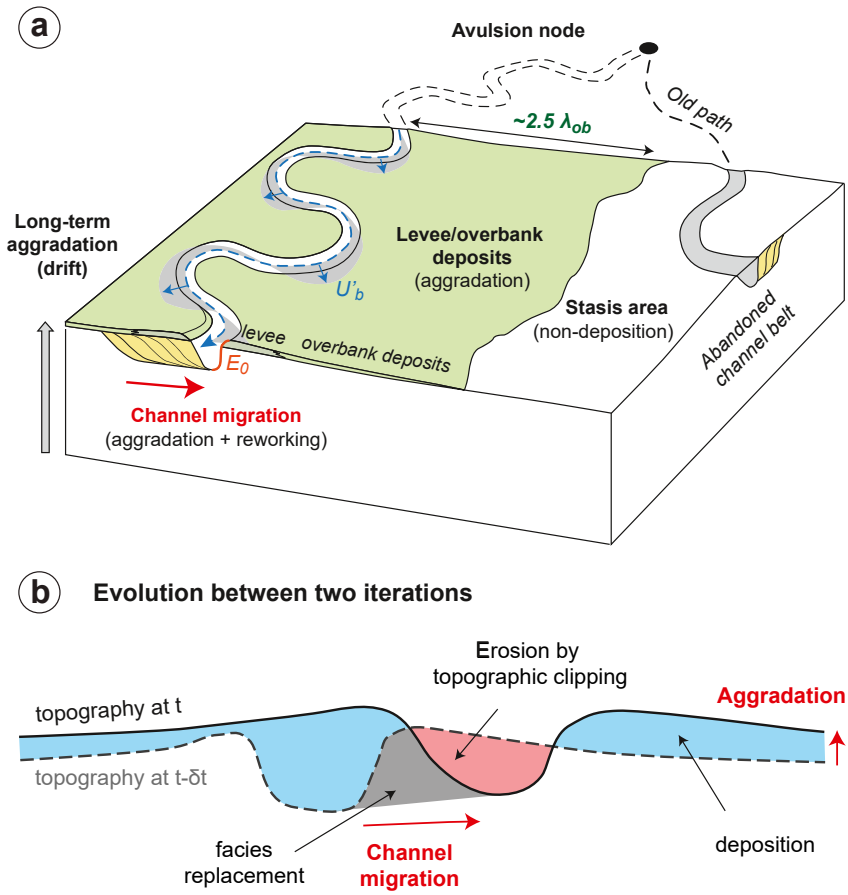

Figure 2. (a) Schematic 3D view of an alluvial meandering system showing the different processes at play: (i) continuous channel migration with associated point bar deposition in the inner bank and erosion at the outer bank, (ii) levee/overbank sedimentation in the floodplain (as well as area of non-deposition or stasis), and (iii) switch of depositional area following avulsion. U'_b is the velocity perturbation and E_0 is the erodibility coefficient at the bank (See Supporting Information. (b) Detail of strata and topographic evolution (cross section) in between two iterations. Note that the gray area corresponding to facies replacement would not be captured by a simple clip between the two topographies.

measure $V_{\delta t}$ evolution with time from 2D data, for instance building synthetic stratigraphy using successive timed topographies of experiments (e.g., Straub & Foreman, 2018). Measure of $V_{\delta t}$ from topographic changes alone are however underestimated (see Figure 2b) and must be complemented with the record of deposit replacement (~ facies replacement).

The completeness $C_{\delta t}$ of a stratigraphic section is the fraction of time intervals of duration δt that left a record (Sadler & Strauss, 1990) and is expressed as the number $n_{\delta t}$ of intervals leaving a record divided by the total number of intervals $N = T/\delta t$ (Figure 1).

$$C_{\delta t} = \frac{\delta t\, n_{\delta t}}{T} = \frac{n_{\delta t}}{N} \tag{2}$$

Sadler (1981) and Sadler and Strauss (1990) demonstrated that completeness increases as a function of (a) the duration of the section (difference between age of the bottom and top of a section), (b) the time span at which a record is discretized and (c) the long-term accumulation rate (referred to as the drift; Figure 1a), and decreases as a function of the unsteadiness of depositional processes. These authors summarized it as the ratio of the long-term accumulation rate A_T (measured over T) to the shorter-term accumulation rate $A_{\delta t}$ (measured with time span δt). Based on a compilation of thousands of accumulation rates, Sadler (1981) also expressed $C_{\delta t}$ as follow:

$$C_{\delta t} = \frac{A_T}{A_{\delta t}} \tag{3a}$$

Introducing $m = \mathrm{d}(\ln A_T)/\mathrm{d}(\ln T)$, a gradient or scaling exponent characteristic of each depositional environment, which varies between -1 and 0, Equation 3a yields:

$$C_{\delta t} = \left(\frac{\delta t}{T}\right)^{-m} \tag{3b}$$

where $\delta t/T$ is the record precision. This scaling exponent m is thus that of the power law function relating measured accumulation rates with time span of measurement. For alluvial environments, m is comprised between -0.5 and -1 (Paola et al., 2018; Sadler & Jerolmack, 2015).

Finally, surface fluctuations driving the Sadler effect can be described as a Brownian fractional motion with positive jumps representing deposition, negative jumps representing erosion and the Hurst exponent h the correlation structure between negative and positive jumps (see references in Paola et al., 2018). Under this assumption, Schumer et al. (2011) demonstrated that h can be related to the scaling exponent defined by Sadler (1981) ($m = h - 1$). When h is 0.5, fluctuations mimic a pure random walk and no correlation can be found between positive and negative jumps. If $h > 0.5$, the motion is persistent and an either decreasing or increasing trend may be observed while if $h < 0.5$ the motion is anti-persistent and jumps are negatively correlated (positive jumps most often follow negative jumps and vice versa).

Most studies have stressed the importance of stasis S and reworking R in setting completeness. R can be defined as the ratio of the sediment lost (eroded) to the sediment gained (deposited) while S is the areal fraction without deposition over the considered domain. Both are measured at a time resolution δt. A simple mathematical expression of their relationship with completeness is the following proposition:

$$C_{\delta t} = (1 - S_{\delta t})(1 - R_{\delta t}) \tag{4}$$

This formulation can be thought of as the "glimpse of a glimpse" preserved in stratigraphy (Holbrook & Miall, 2020). The first term $(1 - S)$ would represent the area not in stasis (i.e., deposition) while the second $(1 - R)$ would represent the sediment that does not get reworked (i.e., preservation). This new formulation for quantifying completeness will be tested against synthetic data generated with FLUMY.

3. Methods

Alluvial deposits of meandering rivers were generated using the FLUMY software. The deposits were analyzed using Python scripts to measure completeness, stasis, accumulation rates and reworking (Figures 2–9). Results were compared with existing formulations of completeness (see previous section).

3.1. Alluvial Deposits Simulations

The FLUMY model combines a pseudo-1D description of channel lateral migration together with parametric generation of associated fluvial processes (e.g., aggradation and avulsion). A detail description of FLUMY can be found in Supporting Information S1. The channel is discretized in a series of nodes representing the centerline. Channel migration rate is calculated at each node of the centerline based on the pioneer bank instability model of Ikeda et al. (1981), adapted by Johannesson and Parker (1989), and many others (e.g., Eke et al., 2014; Howard, 1996; Imran et al., 1999; Parker et al., 2011; Seminara, 2006; Sun et al., 1996) -including Lopez (2003) in the case of FLUMY (Figure 2a). The conservation of channel bankfull mean aspect ratio $2\,B/H$ was assumed based on existing literature compilations (Held, 2011; Lemay et al., 2020; Leopold & Wolman, 1960; Richards, 1982; Williams, 1984, 1986). Fluvial mean bankfull channel depth H, maximum bankfull channel depth $H_{\max}$ and mean bankfull channel width W were related using:

$$W = 2B = 15H = 10\,H_{\max} \tag{5}$$

These average relationships were chosen for they simplicity, keeping in mind that (a) they may be more diverse in nature depending on climate or vegetation (Lemay et al., 2020 after Held, 2011) and that (b) they may be modified in FLUMY depending on the settings.

In FLUMY, deposits are stored according to lithofacies (Table 1) in the domain, a regular 2D pillar grid. To avoid numerical edge effects related to channel migration on the sides, the simulated domain is larger

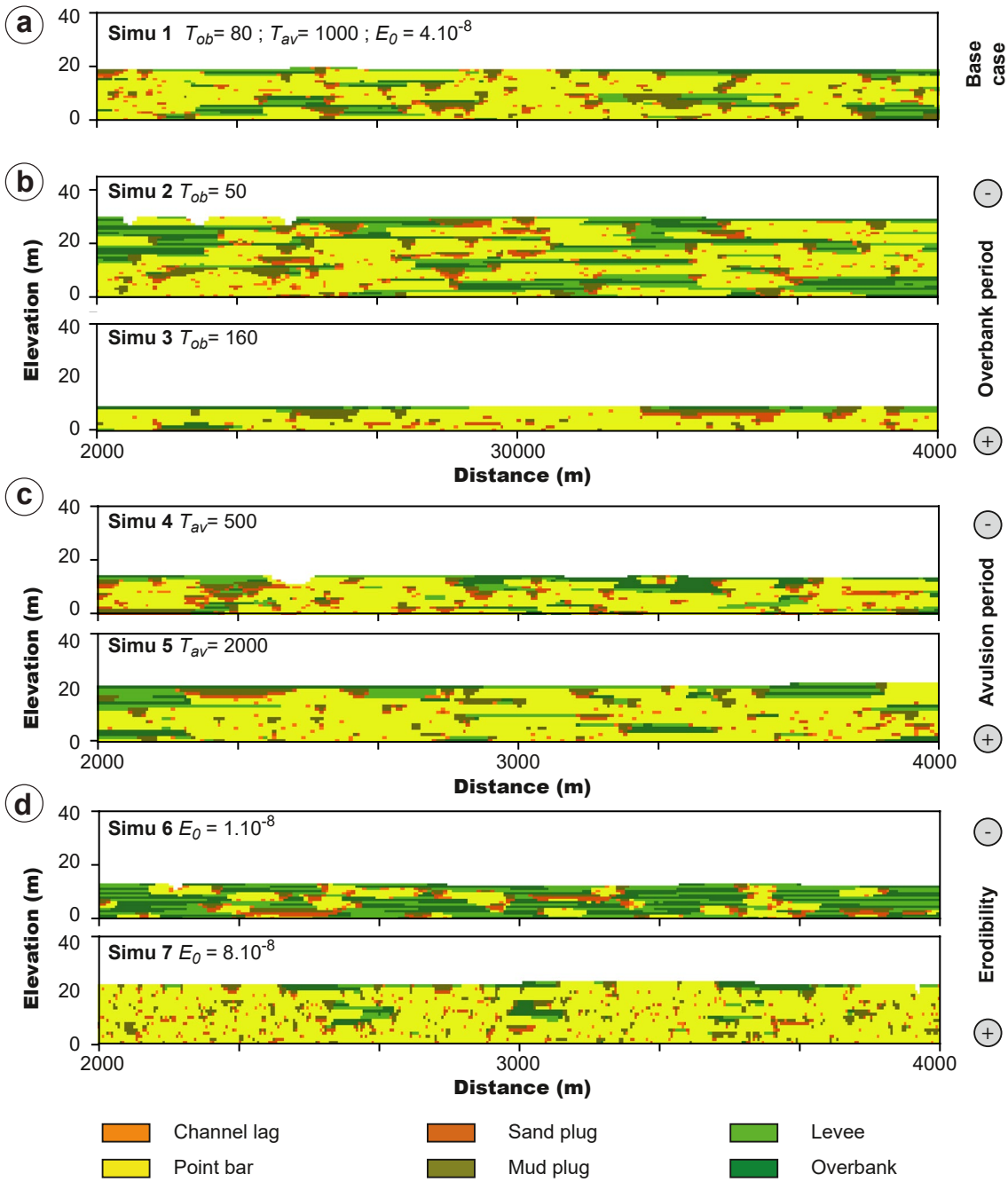

Figure 3. Cross-sectional view (xz at $y = 75$) of facies distribution resulting from the different scenarios tested in this study: (a) base case, (b) varying aggradation rate, (c) varying avulsion period, and (d) varying bank erodibility E_0. See Table 2 for parameters. T_{ob} is the time-span between successive levee/overbank deposition events, and T_{av} between successive avulsion events.

than the domain where facies are saved. *Point Bar* facies (Table 1) are deposited along the inner bank of the channel during lateral migration and allow the adjustment of channel width to erosion on the opposite bank (Figure 2a). Overbank flood geometry is simulated using an exponential thickness decrease away from the channel (Lopez, 2003; Pizzuto, 1987) set by the following input parameters: (a) an initial maximum thickness of overbank deposits i_{ob} and (b) a lateral extension-decrease length of overbank deposits λ_{ob} (Figure 2a) (Supporting Information S1). Overflow events occur following an overbank period T_{ob}, which is also set by the user. *Levee* deposits are generated from the channel to a distance set by the user where they transition to *Overbank* deposits. Note that since FLUMY does not explicitly models flow spilling from the channel, there

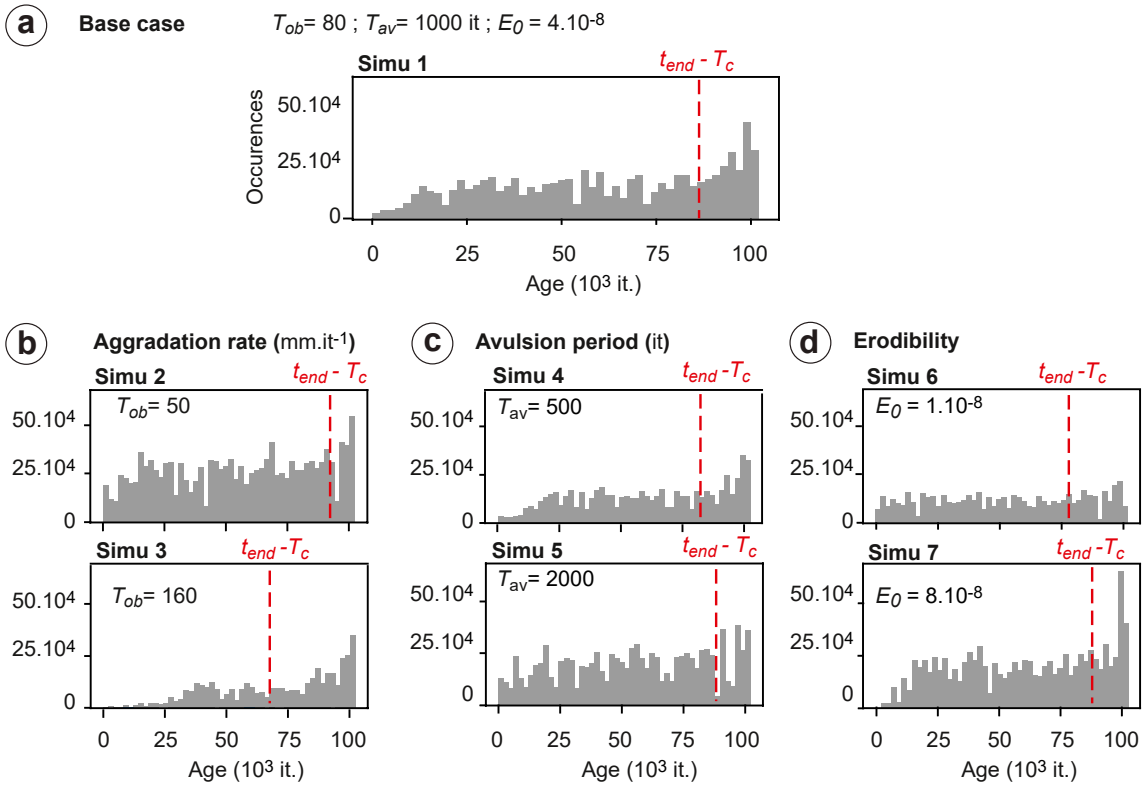

Figure 4. Age distribution of deposits along the cross-sections shown in Figure 3. The red dashed line represents the time limit beyond which older deposits are no longer subject to reworking.

is no flood-induced erosion on the floodplain. C*hannel Lag* is deposited at the bottom of the channel, with a thickness equal to the imposed aggradation thickness to maintain channel depth constant. A regional avulsion process is generated (following an imposed period T_{av} between avulsion events) by changing the entire path of the river on the deposition domain (Supporting Information S1). The old channel path is filled by channel fill deposits (*Sand Plug* and *Mud Plug*) in one iteration, which is an oversimplification as it prevents reoccupation.

Table 2 summarizes parameters that varied in the 7 simulated scenarios. Total duration T of simulation was 102,400 iterations. This duration was chosen to avoid artifacts when discretizing into time spans. With a recurrence of flood (i.e., one iteration in the model) considered as 1.5 years from observations of modern fluvial systems (Lopez, 2003), all simulations may be considered as about 150 kyr long.

A 3 m maximum channel depth (Table 2) was used, resulting in channel width of 30 m (Equation 5). For simplicity, we used a strictly periodic generation for aggradation and avulsion processes. A default scenario (base case; T_{ob} = 80 it., T_{av} = 1,000 it., E_0 = 4.10^{-8}) was defined for comparison with other simulations. In the latter, parameters were changed in turn: (a) T_{ob} to 50 and 160 iterations (Simus 2–3), (b) T_{av} between 500 and 2,000 iterations (Simus 4–5) and (c) E_0 to 1.10^{-8} and 8.10^{-8} (Simus 6–7) (Table 2). For each scenario, a compensation timescale T_c was calculated (Table 2) by dividing the maximum channel depth by the long-term accumulation rate A_T.

During a simulation, depositional information is temporary stored in deposition units of various thicknesses (minimum 1 cm thick) and stacked in vertical pillars. The information can be saved regularly in 3D grids. In the present study, *xyz* grid were 600 × 150 × 200 with a 10 × 10 × 0.2 m discretization (resulting block was thus 6,000 m perpendicularly to flow direction, 1,500 m in the flow direction and 40 m thick). Overbank parameters i_{ob} and λ_{ob} were set at 0.1 ± 0.03 m (normal distribution used in this study, although it can be set to be uniform or log-normal by user) and 450 m, respectively. The resulting levee-overbank extension was thus 1,125 m at maximum (Figure 2a, thickness = 1 cm for 2.5 λ_{ob}). The simulation domain was then larger than the floodplain,

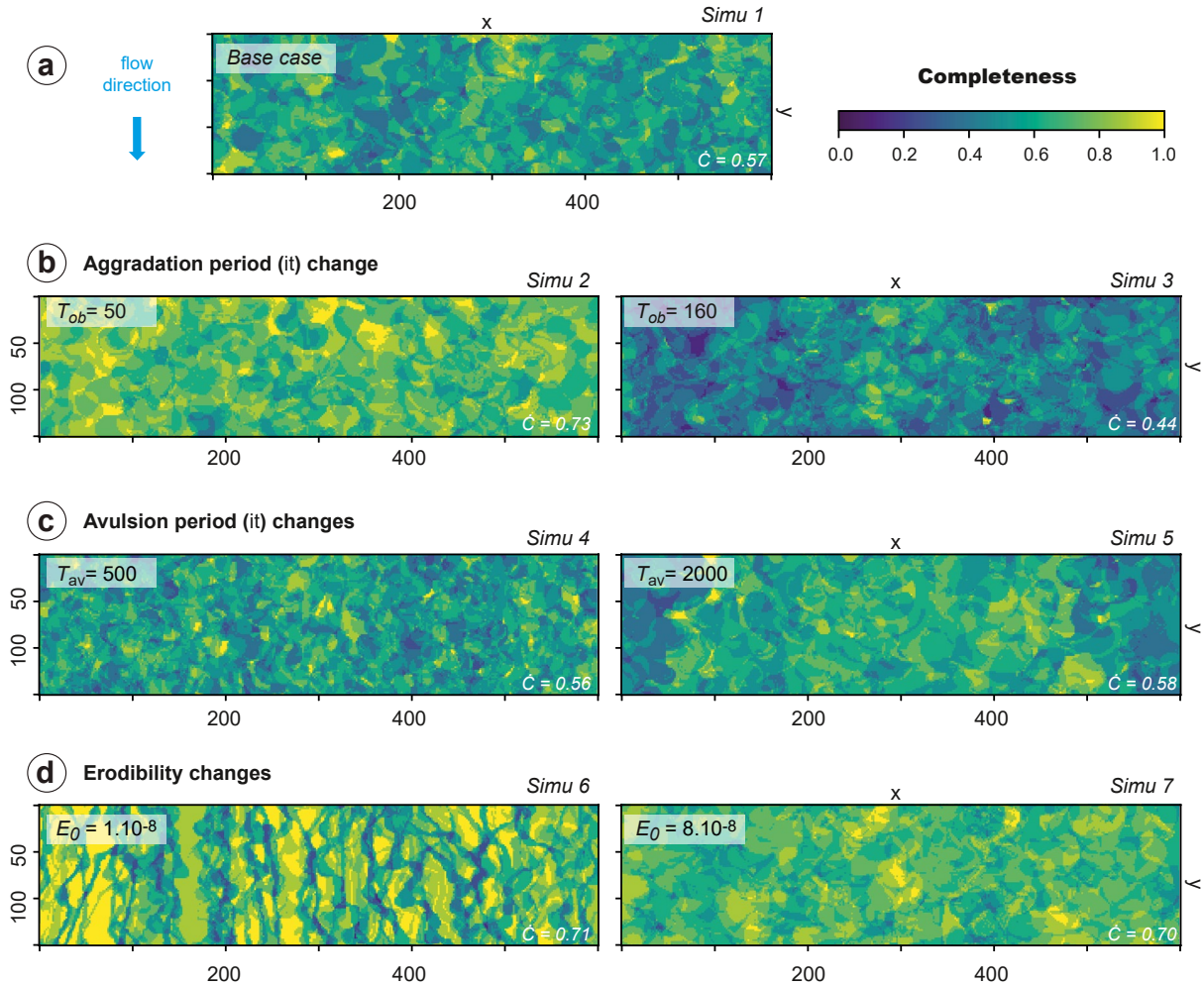

Figure 5. Map (x,y) view of computed completeness values measured at δt = 6,400 iterations for the (a) base case, (b) varying aggradation rate, (c) varying avulsion period, and (d) varying bank erodibility scenarios. Average completeness over the domain $\dot{C}$ is indicated.

which would correspond to the distal part of large alluvial fans to the proximal part of deltaic systems. Note that for a default value of 30 m for channel width (Equation 5), the 2D (map) grid resolution was 0.34 W; that is, finer than the value of 0.4 W, above which unexpected threshold effects related to grid resolution occur (Limaye & Lamb, 2013).

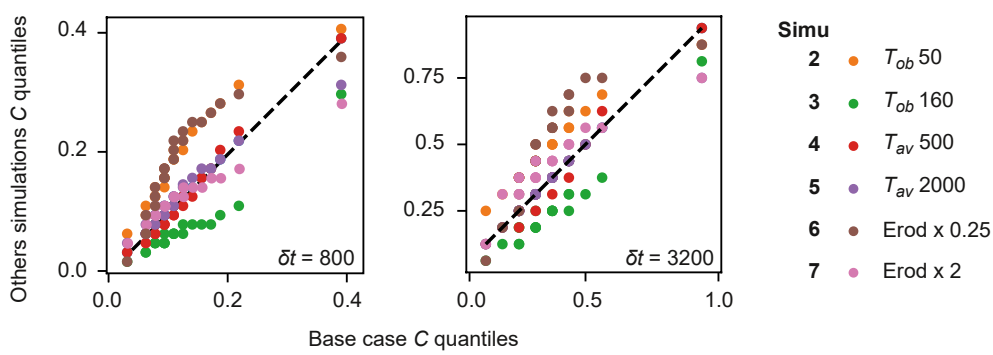

Figure 6. Q-Q plots of completeness values comparing scenarios with the base case (δt = 800 and 3,200 iterations). See Table 2 for parameters.

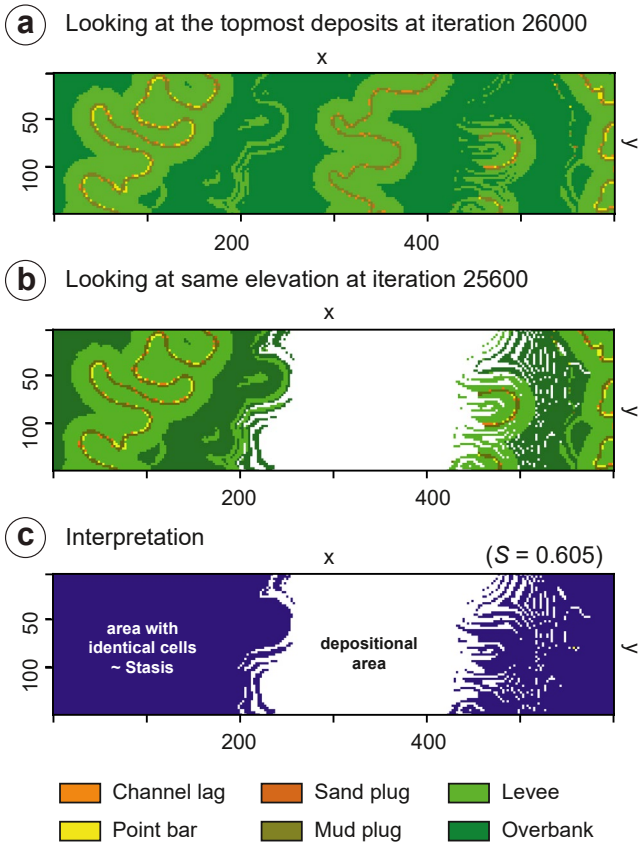

Figure 7. Map (x,y) view showing steps in measuring stasis: a comparison is made between the deposit at the topmost cell of a given 3D grid (a) and the same elevation some δt iterations before panel (b). Stasis corresponds to the number of cells that did not change between the two grids (c) divided by the total amount of cells (x.y). See methods for details.

3.2. Measurements and Comparison With Theory

Alluvial deposit evolution was monitored by saving a 3D grid of the evolving facies every 200 iterations, a period longer than T_{ob}. Deposit type (Table 1) was saved in each grid while the "age" (i.e., iteration of deposition) of preserved deposits was also saved in the final grid (i.e., iteration 102,400). Figure 3 shows the final arrangement of the deposits for all scenarios along the cross-section (xz) located at the 75th y-node of the grid while Figure 4 shows the age distribution of the preserved deposits along the same section. Computation of completeness (that will be denoted by the variable C), stasis, reworking and accumulation rates (Figures 5–11) were made in the interval between 25,600 (to generate a deposition substrate of thickness nearly equivalent to one channel depth) and 76,800 iterations (to exclude the last deposits, less affected by erosion (see Figure 4).

3.2.1. Completeness

Ages of deposits at the final (102,400th) iteration were used to calculate stratigraphic completeness based on Equation 2 for each time span (200; 400; 800; 1,600; 3,200; 6,400; 12,800; 25,600 and 51,200). $C(x,y)$ maps were computed for the different forcing scenarios (see Figure 5 for δt = 6,400). C values distribution were compared using Q-Q plots on 900 values by sub-sampling the grids every 10 nodes (Figure 6).

3.2.2. Stasis

S was calculated by comparing pairs of 3D grids with spacing δt (i.e., computing on all possible pairs and returning the average). First, the elevations and facies type of the topmost deposits were identified for the youngest 3D grid (at t; Figure 7a). Second, the corresponding cells were compared with that of the oldest 3D grid (at t- δt; Figure 7b). Stasis corresponded to the proportion at the surface of the map where t and t- δt cells were identical (Figure 7c), that is, no change was observed. Because the system is aggrading at the timescale of 3D grids extraction, there is no configuration where pure facies replacement occurs—that is, without deposition above- and that could be confused with stasis (Figure 8). It is exemplified in Figure 2b: there is always levee deposits observed above point bar deposits.

3.2.3. Accumulation and Reworking

Changes in facies were measured similarly to stasis, that is, by comparing the cells of the 3D grids between t and t- δt. Apart from the cells that did not change between iterations (see above), three cases were considered: (a) going from nothing to a deposit was counted as deposition (*depo*), (b) going from a deposit to nothing was counted as erosion (*erod*) and (c) changing the deposit type was counted as facies replacement (*fr*) (Figure 2b). It was possible from these measurements to visualize how changes in the depositional record evolved as a function of δt. It is illustrated in Figure 9, where *fr* and *erod* in Simu 2 are plotted as a fraction of deposition (*depo* + *fr*); the remaining part corresponding to preservation.

R was measured as the sum of cells with erosion and facies replacement divided by the sum of cells with facies replacement and deposition (summed on all pairs with spacing δt):

$$R_{\delta t} = \frac{\sum_{j=1}^{N} (erod_{\delta tj} + fr_{\delta tj})}{\sum_{j=1}^{N} (fr_{\delta tj} + depo_{\delta tj})} \quad (6)$$

Resulting values of R were plotted, together with C and S as a function of δt (Figure 10).

Finally, the short-term accumulation rate was computed using Equation 1 in two different ways: one that measured topographic changes alone ($A_{\delta t}$) and one that also included facies replacement ($A_{\delta t}^{*}$) (Figure 11).

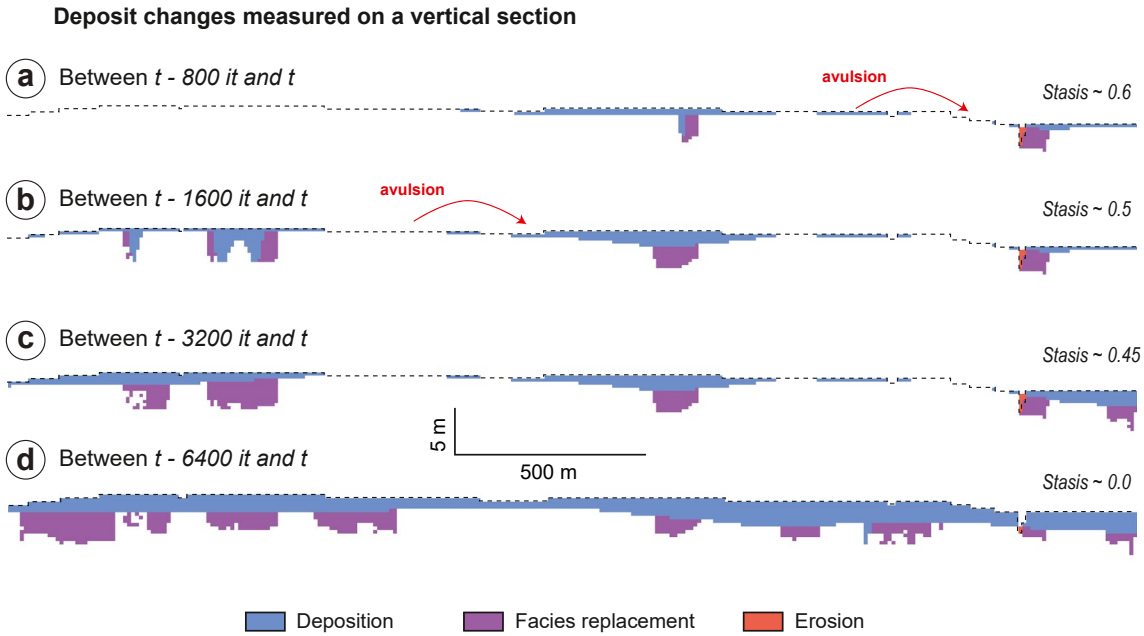

Figure 8. Cross-sectional view (xz at $y = 75$) of deposits changes between 3D grids measured in Simu 2 for increasing δt (from 800 to 6,400 it.). The 3D grid was saved at 25,600 it (iteration t). Comparisons between (a) t-800 and t, (b) t-1,600 and t, (c) t-3,200 and t, and (d) t-6,400 and t illustrate the spatial distribution of facies replacement, deposition and erosion. See methods for details.

$$A_{\delta t} = \frac{\sum_{j=1}^{N} (depo_{\delta tj} - erod_{\delta tj})}{TD\,(1 - S_{\delta t})} \tag{7}$$

$$A_{\delta t}^{*} = \frac{\sum_{j=1}^{N} (depo_{\delta tj} - erod_{\delta tj} + fr_{\delta tj})}{TD\,(1 - S_{\delta t})} \tag{8}$$

$A_{\delta t}$ included deposition (*depo*) less erosion (*erod*) while $A_{\delta t}^{*}$ included deposition less erosion and facies replacement (*fr*). D denotes the area of the 2D domain considered (see Supporting Information S1 for a detailed description).

3.2.4. Comparison With Existing Theory

Boxplots of completeness calculated from all simulations were plotted against their theoretical predictions in Figure 12. These included Equation 3a using either $A_{\delta t}$ or $A_{\delta t}^{*}$ (Figure 10d), Equation 3b using either m = d (ln A_T)/d (ln$T$)—which returned values of -0.8 ± 0.05 - (Figure 10c) or $m = -0.5$ (Figure 10b), and Equation 4 (Figure 10e). T_c, that is, the limit where the Sadler effect saturates, was used instead of T to calculate precision. Finally, theoretical predictions for C using Equation 3a with $A_{\delta t}^{*}$ and Equation 4 were plotted against each other for comparison.

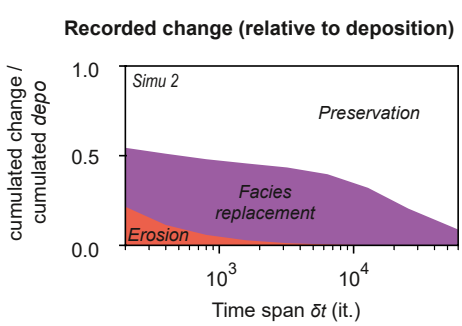

Figure 9. Record of facies change measured as a function of δt expressed relative to deposition: example of Simu 2. Note that erosion becomes negligible when measured over 3,000 iterations.

4. Results and Interpretations

4.1. Deposit Architecture and Age Distribution

The seven simulations tested in this study showed contrasted sedimentary architectures in response to parameter changes (Lopez et al., 2009) (Figure 3). Increasing aggradation rate (by reducing T_{ob}) leads to higher final elevations (Table 2) and increase in proportion of overbank deposits compared to channelized deposits (Figure 3b). Decreasing avulsion period leads to increased channel abandonments and associated channel-fill deposits, but

Table 1
Deposit Types Used in the Simulations and Associated Processes

Location	Deposit facies	Associated process
Overbank flooding area	Overbank	Fine (silt-clay) deposition mostly by decantation after flood
	Levees	Rapid settling of suspended sediments flooding out of the channel as a result of decreasing turbulence
Channelized deposits	Mud Plug	Fine-grained fraction of abandoned channel fill
	Sand Plug	Coarse-grained fraction of abandoned channel fill
	Point Bar	Fining-up, usually sandy deposits accumulating in the inner bend of channel as it migrates
	Channel Lag	Coarse deposits associated with high transport capacity at the bottom of channel

also to narrowed point bar due to abandonment occurring before the establishment of high sinuosity channels (Figure 3c). On the contrary, increasing bank erodibility favored lateral migration of channels, which increased the proportion of point bar deposits (Figure 3d).

Age distributions of the preserved deposits varied depending on the simulated scenarios, although some similarities were observed (Figure 4). In all scenarios, the time interval that has a maximum time preservation was found at the end of simulations, between (t_{end}-T_c) and t_{end}. It is best exemplified in simulations with either low accumulation rate (Simu 3), high avulsion rate (Simu 4) or high erodibility (Simu 7). Before t_{end}-T_c, age distribution was also heterogeneous in most scenarios with large fluctuations (Figure 4). It was sometimes observed that these fluctuations scaled with T_c such as in Simu 1 where about six fluctuations were identified (Figure 4a), or in Simu 5 where about seven fluctuations were observed (Figure 4c). Age distributions in all simulations were thus consistent with theory on compensation timescale and further validated the choice not to include the youngest deposits in estimating C, R and S, as these "younger" deposits were better preserved than the other ones.

4.2. Distribution and Evolution of Completeness

Completeness maps showed heterogeneous distribution in space, as illustrated on Figure 5 by the maps at $\delta t = 6{,}400$. C values were more spatially variable in cases with low erodibility (Simu 6) or short overbank flow period (Simu 2) (Figures 5 and 6). In the case with low bank erodibility (Figure 5d; Simu 6), the sinuous channel shapes correspond to low values of C, separated by high values of C of preserved overbank deposits in areas that had not been swept by the channel thanks to the limited migration.

Comparisons of C distributions with the base case showed that simulations with high aggradation rate or low erodibility (Simus 2 and 6) typically had a higher dispersion and median value, compared to simulations with low aggradation rate or high erodibility (Simus 3 and 7) (Figure 6). Simu 7 crossed the $y = x$ line, likely because of a

Table 2
Parameters Varied in the Simulations and Resulting Series Characteristics (Z_{end}, A_T and T_c)

Simu	Overbank flood period T_{ob} (it.)	Regional avulsion period T_{av} (it.)	Erodibility coefficient E_0	Section age t_{end} (it.)	Mean final elevation Z_{end} (m)	Acc. Rate (m/it.) $A_T = Z_{end}/t_{end}$	*Compensation* timescale (it.) $T_c = H_{max}/A_T$
1-Base case	*80*	1000	$4.00\ 10^{-8}$	102,400	18.73	$1.83\ 10^{-4}$	16,400
2- Aggrad50	50	1000	$4.00\ 10^{-8}$	102,400	29.45	$2.88\ 10^{-4}$	10,432
3-Aggrad160	160	1000	$4.00\ 10^{-8}$	102,400	8.78	$8.57\ 10^{-5}$	34,990
4-Avuls500	80	500	$4.00\ 10^{-8}$	102,400	14.33	$1.40\ 10^{-4}$	21,434
5-Avuls2000	80	2000	$4.00\ 10^{-8}$	102,400	21.82	$2.13\ 10^{-4}$	14,080
6-Ero0.25	80	1000	$1.00\ 10^{-8}$	102,400	12.34	$1.20\ 10^{-4}$	24,898
7-Ero2	80	1000	$8.00\ 10^{-8}$	102,400	21.84	$2.22\ 10^{-4}$	13,488

Note. 3D grids were saved every 200 iterations.

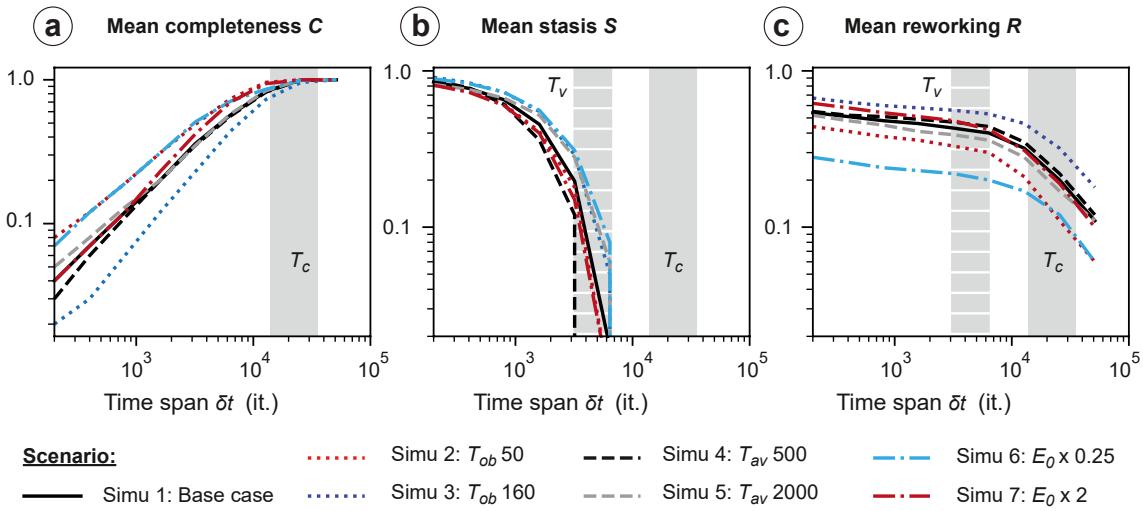

Figure 10. (a) Mean completeness, (b) stasis, and (c) reworking shown for all simulations as a function of δt. T_c and T_v correspond to compensational and visitation timescales, respectively.

bimodal distribution of values. Simulations with changing avulsion period had C distributions comparable with that of the base case. C median values overall increased with δt without significantly altering this trend (Figure 6).

All curves of mean completeness as a function of δt had similar shapes (Figure 10a). Mean completeness started at ~0.1 for $\delta t = 200$ and increased with δt and equal one when measured for $\delta t > T_c$ (Figure 10a). On average, Simu 3 (low accumulation rate) had the lowest completeness while Simu 2 (high accumulation rate) had the highest completeness. For δt values higher than 200, C increased rapidly for Simu 7 to reach values like that observed in Simu 2.

4.3. Surface Evolution Related to Channel Motion

The stasis fraction started around 0.8 for $\delta t = 200$ and decreased as a function of δt (Figure 10b). Around $\delta t = 1{,}000$ –which corresponded to T_{av} in most simulations except Simus 4 and 5- the decrease of S was faster. This likely illustrated the start of avulsion that greatly enhanced visitation of the floodplain by new channel path and associated overbank deposits. S went down to zero for δt above 3,000–17,000 iterations depending on simulations. We defined this threshold, which roughly corresponded to 6–10 avulsions depending on the scenario, as the timescale T_v of visitation of the entire domain by overbank sedimentation (Figure 8). Overall, S did not vary by more than 25% between simulations. A high stasis fraction was observed for simulations with long T_{av} (Simu

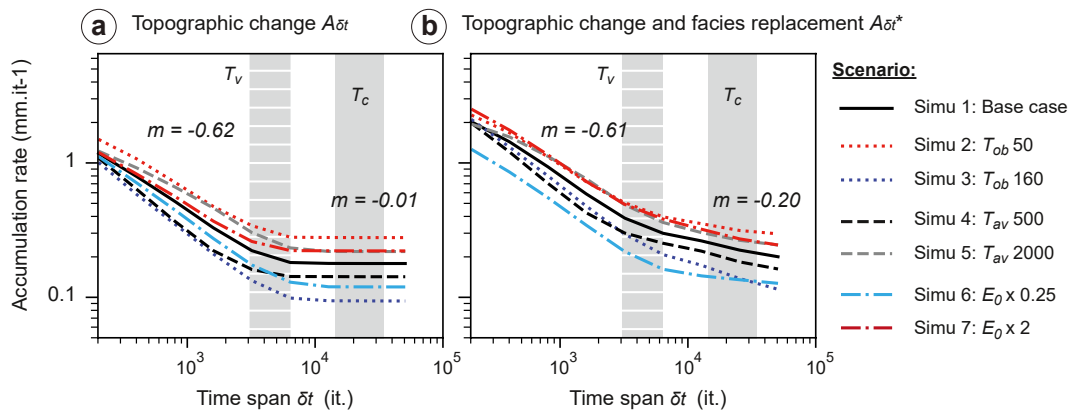

Figure 11. Short-term accumulation rates $A_{\delta t}$ and $A_{\delta t}^*$ for each simulation as a function of δt. T_c and T_v correspond to compensational and visitation timescales, respectively.

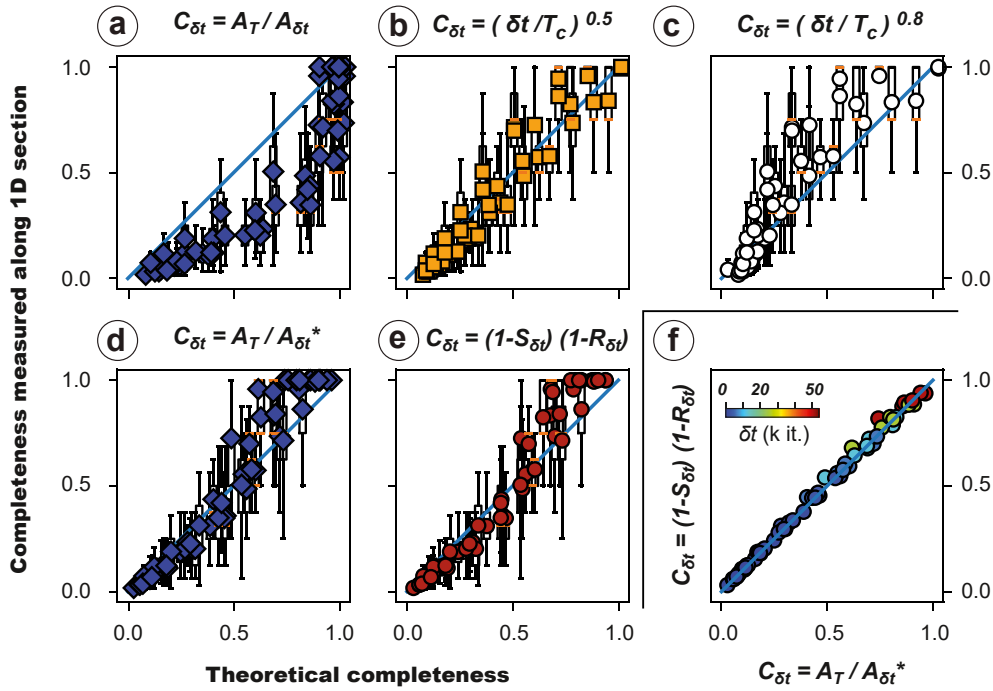

Figure 12. Comparison between the distributions of completeness values (boxplot) measured from simulations and estimates from theory. (a–d) are from Sadler (1981) (e) from this study while panel (f) is a cross plot between the theoretical predictors in panels (d) and (e).

5), low erodibility (Simu 6), or long T_{ob} (Simu 3). Finally, Figure 10 shows that completeness C and stasis fraction S had opposite trends, suggesting an inverse coupling between the two parameters (i.e., Tipper, 2015).

Figure 8 shows that facies replacement and erosion were mostly measured in the lowest part of sections - corresponding to the migration of the active channel incising the floodplain and depositing point bars - while deposition was located at the top, corresponding mainly to levee and overbank deposition. Erosion was small as it corresponded to the channel volume and kept a fairly constant value through time (albeit depending on channel sinuosity) (Figure 8). Facies replacement increased with δt but much slowly than deposition. With increasing δt, the fraction of erosion and facies replacement that could be recorded relative to deposition thus decreased (Figure 9), and R also mechanically decreased (Figure 10c).

Figure 9 shows that for Simu 2 at $\delta t = 200$, about 20% of *erod* and 40% of *fr* relative to *depo* could be measured, that is, an equivalent R of 0.4 (Figure 10c). The ability (proportion) to measure erosion (channel volume) vanished exponentially with δt so that it was close to zero when measured using δt over 4,000 it (Figure 9). After that timescale, the ability to measure reworking was available through facies replacement only. Overall, R slowly decreased with increasing δt until a break is observed around 5,000–15,000 it. and the decrease was faster (Figures 9 and 10c). The break corresponded to T_v, that is, stasis was then zero (Table 2). This behavior was observed in all simulations although the mean value of R varied by a factor of 2–3 between simulations. R values were low for low erodibility coefficient (Simu 6) and low overbank period (Simu 2), and high for large overbank period (Simu 3) (Figure 10c).

Measured short-term accumulation rates $A_{\delta t}$ and $A_{\delta t}^*$ decreased with increasing δt and looked very similar between the different simulations (Figure 11). Simu 7 (with high erodibility) had an accumulation rate similar to that of Simu 2 (i.e., low T_{ob}). The value of $A_{\delta t}$ was lower than $A_{\delta t}^*$. Both $A_{\delta t}$ and $A_{\delta t}^*$ curves showed a break around T_v (Figure 11). They both converged toward a similar value, which corresponded to A_T, although it was attained much more rapidly (at T_v) in the case of $A_{\delta t}$. In the case of $A_{\delta t}$, power law fits of the two segments of the curve in the 200–3,200 and 6,400–51,200 intervals returned exponents of −0.62 and −0.01 respectively while a fit in the 200–51,200 interval returned −0.44 (Figure 11a). In the case of $A_{\delta t}^*$, power law fits of the two segments of the

curve in the 200–3,200 and 6,400–51,200 intervals returned exponent of −0.61 and −0.20 respectively while a fit in the 200–51,200 interval returned −0.44 (Figure 11b).

4.4. Predicted vs Measured Completeness

A comparison was made between the results of this study and existing theory on completeness (Figure 12). The first striking result was that C was better estimated when using Equation 3b of Sadler (1981) with $A_{\delta t}^{*}$ (Figure 12d) than topographic change only $A_{\delta t}$ (Figure 12a). In detail, the former was an especially good predictor for value of C lower than 0.5 and more variable for values of C above 0.5. For estimations using the precision $\delta t/T$, a better agreement was observed when using $m = -0.5$ (Figure 12b) instead of $m = -0.8$ (Figure 12c), suggesting that m is close to −0.5. In the latter, the theory seemed to underpredict measurements from the simulation (Figure 12c). The new Equation 4 relating mean completeness to mean deposition area $(1 - S)$ and the mean preserved deposits $(1 - R)$ was in good agreement with measurements (Figure 12e). Finally, a cross plot between the theoretical estimates in Figures 12d and 12e, which were rather good predictors, was presented in Figure 12f. It showed that the two formulations have very similar outcomes, although some slight variability was observed for the values of C above 0.5.

5. Discussion

In this study, it was possible to track both topographic and sediment changes associated with fluvial meandering dynamics, that is, complementing works that mainly tracked topographic changes in physical experiments (Straub & Esposito, 2013; Straub & Foreman, 2018) or numerical simulations (e.g., Durkin et al., 2017; Wang et al., 2021; Yan et al., 2021). Results show that this combination of topographic and facies replacement measurement allows for a better prediction of completeness than topographic data alone (comparison between Figures 12a and 12d).

5.1. Anti-Persistent and Persistent Regimes

In the present study, several thresholds are identified. For instance, the avulsion timescale corresponds to an accelerated decrease of S. Another threshold is perhaps reached when the ability to track erosion is low (Figure 9). The compensation timescale T_c corresponds to the transition where C equals one (Figure 10a). T_v (i.e., the timescale from which $S = 0$) corresponds to breaks in short-term accumulation rate (Figure 11) and R (Figure 10c) decreases as a function of δt.

Similarly to previous studies, a decrease of accumulation rates $A_{\delta t}$ with the time span δt is shown. A power-law fit of $A_{\delta t}^{*}$ versus δt (Figure 11) over the whole δt range returned an exponent m close to −0.5 (i.e., −0.44 with $R^2 = 0.85$). Using $m = -0.5$ rather than the empirical one found by Sadler (1981) (ca. −0.8 for fluvial data) allowed a rather good prediction of mean observed C (Figures 12b and 12c). According to Schumer et al. (2011), this suggests that the surface evolution in the model could be described as a Fractional Brownian motion ($h = 0.5$). This means that topographic fluctuations building the stratigraphy worked as if positive and negative jumps were uncorrelated, which would correspond to a random walk. Such result is surprising as the parameters used in the model were set so that stochasticity was limited. Overall, this can tentatively be explained by the variety of (fluvial) processes at play in the model.

In detail, the changes in the rate of $A_{\delta t}^{*}$ decrease with δt allows distinguishing between a non-persistent (when $\delta t < T_v$) and a persistent regime (when $\delta t > T_v$). Before T_v, m is −0.62, which mean that h is between 0 and 0.5 (Schumer et al., 2011). This indicates that the jumps are negatively correlated, suggesting a regime typically dominated by compensational stacking (Straub & Esposito, 2013; Straub et al., 2009). In this regime, channel motion –i.e., by avulsion-is influenced by levee topography (Figures 2 and 8). Sedimentation is then more likely to occur in topographic lows where sediment has not deposited yet (Pelletier & Turcotte, 1997). Thus $A_{\delta t}^{*}$ decreases very fast with δt. When measured beyond T_v, $A_{\delta t}^{*}$ keeps decreasing, although much slowly. The power-law exponent m is −0.2; therefore h is between 0.5 and 1, which reveals persistence phenomenon (Jerolmack & Sadler, 2007). In this regime, a positive correlation between elevation jumps is found, which supposes that an area receiving sediment is more likely to receive sediment at the next step. This is consistent with stasis being zero and accumulation being recorded everywhere in the domain at such timescale (Figure 8d). Only after T_v can

then accumulation be considered as a drift in the sense of ubiquitous deposition. Reworking related to channel migration is then the unsteady surface process. $A_{\delta t}^{*}$ then converges toward A_T.

5.2. Stasis Dynamics

Simulations showed that stasis strongly impacted the value of completeness as pointed out by many authors (Paola et al., 2018 and references therein). Indeed, as shown above, the timescale T_v beyond which S equals zero corresponds to a major change in accumulation dynamics (Figure 11). This is further attested by an (inverse) similarity of the shapes of C and S curves (i.e., Figures 10a and 10b). The strong (anti) correlation between C and S is perhaps best shown by Equation 4 (Figure 10d). Recently, following Tipper (2015), Straub and Foreman (2018) have illustrated the importance of stasis in the value of C, although no direct relation has been proposed yet. The present study allows for a quantification of the importance of this phenomenon.

The timescale T_v used in this study for overbank visitation of the entire domain is similar to the channel timescale necessary to occupy a substantial fraction (e.g., >90%–95%) of a sedimentary basin (Cazanacli et al., 2002; Kim et al., 2010). The latter was defined for experimental fluvial system datasets by cumulating overlapping wetted areas of a basin. In these experimental simulations, floodplain aggradation was proportional to channel aggradation. Topography changed by the migration of bedload-rich systems that occasionally spill out during flooding stages, which occurred autogenically (e.g., Scheidt et al., 2016). Apart from the determinism of flooding occurrence and shapes of overbank deposits, the dynamics in FLUMY and tank experiments are however not fundamentally different, and the existing theory developed for channel timescale may well be adapted to assess T_v.

In the simulations, performed over a given domain, stasis is inversely proportional to levee/overbank deposition length, which was roughly constant (~1,125 m). Considering the width of the domain (6,000 m) and overlaps between overbank deposits, about 6–10 avulsions are necessary to occupy the domain, in agreement with observations (Figure 10b). Consistently, values of T_v are respectively lower and higher in cases with shorter and longer avulsion periods (Figure 10b). Some variability is however observed depending on how well channels can sweep across the floodplain between avulsions (i.e., comparison between Simus 6 and 7).

5.3. Reworking Dynamics

Reworking is a process measured at all timescales (Figure 10c). With a lateral migration rate of bends in the order of 0.5–1 m.it^{-1} in average in the simulations, the channel migrate about 100–200 m (i.e., 3.5–7 channel widths) in between extractions of 3D grids. It is a much more efficient reworking than avulsion, which erodes only one channel width at best every 500 iterations. Observed reworked fraction varied between simulations (Figure 10c). It was typically 40%–70% when measured over short time span (i.e., 200 it.), except for Simu 6 (25%) for which erodibility was low. These values thus quantify at centennial scale the potential for storage and release of sediments on floodplains (Métivier & Gaudemer, 1999). They suggest that fluvial sediments have about a 50% chance to be reworked after their deposition in relation with the continuous migration of a channel. This probability remains high (40%) until δt reaches the T_v value when R decreases faster (Figure 10c). Sustained high R values until T_v likely illustrate enhanced reworking by avulsion, which works by carving new channel paths, until the whole domain is occupied—a counterweight for increased overbank sedimentation in FLUMY. Figure 8 indeed shows that before T_v, each avulsion induces erosion of previous deposits by one channel depth. After T_v, measured reworking decrease rapidly but is still observable. A fraction of migrating channel (point bars) located below the levees at the beginning of measurement is indeed always counted as reworking (Figures 7 and 8). It is inherent to the incisional nature of avulsions in FLUMY, who carve the floodplain and are not aggradational, as sometimes observed in natural systems (Mohrig et al., 2000).

In this study, morphologies (channel, levee/overbank deposits) sizes were kept constant. In nature, these morphologies vary with time. One may thus expect that C would be lowered if channel depth was increased—for instance associated with climate change - as deposits would be reworked more deeply. In that case however, both overbank deposit size and avulsion frequency will likely increase, which would tend to increase C. Testing the impact of channel size change, particularly during transience (e.g., Chen et al., 2018), on strata preservation would require further investigation.

5.4. Completeness Related to Channelized and Non-Channelized Processes

Overall, the anti-persistent and persistent regimes respectively result from non-channelized and channelized processes actions on alluvial plains. *C* maps are indeed often organized into clusters of high and low *C* (Figure 5). In cases of short T_{ob} (Simu 2), low erodibility or short avulsion period, the contrast between the values of *C* in these two domains is further enhanced. Areas of higher *C* define surviving areas (see Durkin et al., 2017) that have not been reworked by channel sweep. These surviving areas are well developed in the case of low bank erodibility (Simu 6; Figure 5d), isolated but significantly large in the case of short T_{ob} (Simu 2; Figure 5b) or high bank erodibility (Simu 7; Figure 5d). They correspond to floodplain deposits, which were minimally eroded and are separated by areas of lower *C* swept by channel migration. These patterns are consistent with the preferential preservation of lower-order (here levee/overbank deposits) relative to higher-order (here point bars and channel fill deposits) hierarchical forms (Ganti et al., 2020). In Simu 6 (Figure 5d), the wide range of *C* values – also observed in the associated Q-Q plot (Figure 6)- is due to limited channel migration that favored a ribbon geometry elongated along the main slope. For the other simulations (2 and 7), the contrasts are lower and no specific shape of the high *C* remnants is observed.

The duality between erosive (channelized) and depositional (mainly non-channelized) processes is also present in Equation 4. It is suggested that this formulation is very similar to Equation 3a of Sadler (1981) by the cross plot in Figure 12f, which can also be demonstrated theoretically, especially for values of $\delta t > 1{,}000$ iterations (See Supporting Information S1). A current limitation is that *erod* is very small compared to *fr* and *depo* and its impact on the formulations is difficult to assess (See Supporting Information S1). Nevertheless, Equation 4 appears appropriate to assess how well a signal is recorded on average along fluvial stratigraphic sections. This formulation could well be tested on the field as follow.

First, *S* could be assessed by measuring the ratio of depositional (∼basin) width to overbank deposits width at a given time step. Such estimation is feasible using interpretations of levee-overbank geometry extent on seismic data. Alternatively, depositional width could be estimated using existing models of the decrease in overbank deposit thickness with distance from the levees (i.e., Gross & Small, 1998; Howard 1996; Howard, 1992; Lopez, 2003; Pizzuto, 1987). Second, *R* could be assessed from field data using proxies such as bar preservation based on their geometry and facies (e.g., Chamberlin & Hajek, 2019). An alternative way would be to use Equation 6 with point bar deposits area as *fr*, floodplain deposits area as *depo*, and *erod* neglected (e.g., Figures 8 and 9).

The seemingly chaotic stratigraphic architecture observed in the model fades away when considering the scaling (and thus process) break at T_v in the dependence of accumulation rates to measurement time span (Figure 9). In other word doing a regression fit of accumulation over the whole range of measurement time spans, which returns *m* close to −0.5, is surely an oversimplification. Nevertheless, it remains striking that completeness measured in the synthetic stratigraphy can be approximated assuming a chaotic construction (Figure 12b). The example of such "chaos arising from order" (Chris Paola, personal communication 2020) highlights that breaks in scale related to geological process may be found, which would allow retrieving information on depositional systems dynamics. For instance, the fact that *m* is −0.585 for alluvial data (Paola et al., 2018; Sadler & Jerolmack, 2015) implies dominance of compensational stacking. In fluvial systems however, and it may not be incompatible, other breaks in scaling including for instance external forcings such angular unconformities driven by tectonic deformation or change of river mobility or size driven by climate may exist. Using different parameterization in FLUMY, for example, allowing local avulsions to occur within the depositional domain or forcing topographic deformation by tectonic processes, could potentially have changed the shape of the dependence of accumulation rate to measurement time span.

5.5. Limitations of the Approach

Although consistent with the general theory, the present results particularly apply to meandering systems, which are less represented than distributive fluvial systems in nature (Weissmann et al., 2015). Results could however be tested in other contexts, for instance in aggrading turbidite environments where similarities to fluvial systems can be observed (Lemay et al., 2020). Of interest will be how *Tv* and T_c encompass changes in accumulation dynamics there. In fluvial system, avulsion period scales with the time for aggradation to elevate the channel above the levees by one channel depth (Jerolmack & Mohrig, 2007). Aggradation and formation of channel plugs

can however occur rapidly (tens of years) (e.g., Szewczyk et al., 2022) and force avulsion with limited overbank deposition at the scale of the floodplain. Such dynamics of rapid switches compared to aggradation may explain how reworking can be well expressed in alluvial systems (Figure 7c). On the contrary, the reworking might be limited due to important levee aggradation (and thus superelevation) before avulsion in submarine channel belts (Jobe et al., 2020). In that case, the evolution of R with measurement time span would look different than in alluvial systems, which should enhance completeness.

Another limitation is that the size of the domain is relatively small compared to the deposition area, hence hiatus duration is short in the present study. There is therefore a bias toward short hiatus, which is enhanced as simulations run for hundreds of thousands of years compared to tens of millions of years in nature. On the other hand, we chose to extract grid data every 200 iteration, which corresponds to ca. 300 years in nature, so that this study has a limited resolution on lower architectural hierarchies (accretion packages) compared to a recent study by Yan et al. (2021). We do include a comparable degree of complexity at the scale of channel belt, since FLUMY also includes changes of direction of migration and bend cut-offs (Lemay, 2018).

Finally, the fact that no reoccupation is allowed is an oversimplification of the model compared to nature and experiments (e.g., Ashworth et al., 2007; Aslan et al., 1999; Morozova & Smith, 2000). In natural systems, after a rapid disconnection stage associated to sand plug formation (e.g., Szewczyk et al., 2020) abandoned channels are slowly filled ($10^{2–3}$ yrs). This is propitious to reoccupation as old channels remain topographic lows. In the simulations, the stratigraphy was thus built by compensational stacking mainly (Sahoo et al., 2020). If reoccupations were allowed, they would decrease reworking compared to the simulations of this study where a new channel path systematically erodes sediments. On the other hand, it would lengthen the time that some areas remain in stasis, that is, away from reoccupied channel paths. Hence, C values should be affected by allowing reoccupations, but because R and S will be affected too, and it should still be possible to predict C using Equation 4.

6. Conclusion

In this study, the evolution of fluvial meandering river deposits was tracked on a series of numerical simulations by combining measurement of topographic and facies evolution. We found that:

1. Accumulation rate dependence on measurement time span allows distinguishing between an anti-persistent and a persistent regime.
2. The former is characteristic of channel avulsion and compensational stacking until the whole domain is visited by overbank deposition, which corresponds to the timescale T_v when stasis $S = 0$.
3. The latter is related to surface fluctuations by channel continuous migration and the associated erosion of formerly deposited alluvium. As persistence in accumulation is attained, reworking R is the remaining active process until the whole system has aggraded one channel depth (i.e., compensation timescale T_c).
4. Based on these results, the mean completeness C can be approximated using $C_{\delta t} = (1 - S_{\delta t})\,(1 - R_{\delta t})$.

Data Availability Statement

Data are reproducible using this version with the batch files available in Supporting Information S1. Flumy (2019) version 5.906 was used in this study. The FLUMY software can be found here: https://flumy.minesparis.psl.eu/ and activated using an activation number provided by the FLUMY team.

Acknowledgments
We would like to thank the partners that supported this research: ENI, Engie, Exxon, Petrobras, and Shell. This work was motivated by discussions with Chris Paola and David Mohrig. We thank Kyle Straub and two anonymous reviewers, as well as Mikael Attal and the associate editor for detailed comments that greatly improved the manuscript.

References

Abels, H. A., Kraus, M. J., & Gingerich, P. D. (2013). Precession-scale cyclicity in the fluvial lower Eocene Willwood Formation of the Bighorn Basin, Wyoming (USA). *Sedimentology*, *60*(6), 1467–1483. https://doi.org/10.1111/sed.12039

Ager, D. V. (1973). *The nature of the stratigraphical record*. The MacMilliman Press.

Ashworth, P. J., Best, J. L., & Jones, M. A. (2007). The relationship between channel avulsion, flow occupancy and aggradation in braided rivers: Insights from an experimental model. *Sedimentology*, *54*(3), 497–513. https://doi.org/10.1111/j.1365-3091.2006.00845.x

Aslan, A., Blum, M., Smith, N., & Rogers, J. (1999). Contrasting styles of Holocene avulsion, Texas Gulf coastal plain, USA. *Fluvial sedimentology VI*, *28*, 193–209.

Cazanacli, D., Paola, C., & Parker, G. (2002). Experimental steep, braided flow: Application to flooding risk on fans. *Journal of Hydraulic Engineering*, *128*(3), 322–330. https://doi.org/10.1061/(asce)0733-9429(2002)128:3(322)

Chamberlin, E. P., & Hajek, E. A. (2019). Using bar preservation to constrain reworking in channel-dominated fluvial stratigraphy. *Geology*, *47*(6), 531–534. https://doi.org/10.1130/g46046.1

Chen, C., Guerit, L., Foreman, B. Z., Hassenruck-Gudipati, H. J., Adatte, T., Honegger, L., et al. (2018). Estimating regional flood discharge during Palaeocene-Eocene global warming. *Scientific Reports*, *8*(1), 13391. https://doi.org/10.1038/s41598-018-31076-3

Durkin, P. R., Hubbard, S. M., Holbrook, J., & Boyd, R. (2017). Evolution of fluvial meander-belt deposits and implications for the completeness of the stratigraphic record. *GSA Bulletin*, *130*(5–6), 721–739. https://doi.org/10.1130/b31699.1

Eke, E., Parker, G., & Shimizu, Y. (2014). Numerical modeling of erosional and depositional bank processes in migrating river bends with self-formed width: Morphodynamics of bar push and bank pull. *Journal of Geophysical Research: Earth Surface*, *119*(7), 1455–1483. https://doi.org/10.1002/2013jf003020

Flumy (2019). Process-based channelized reservoir models [dataset]. MINES ParisTech/ARMINES: Premium Version (v5.906) [Software]. Retrieved from https://flumy.minesparis.psl.eu/download

Ganti, V., Hajek, E. A., Leary, K., Straub, K. M., & Paola, C. (2020). Morphodynamic hierarchy and the fabric of the sedimentary record. *Geophysical Research Letters*, *47*(14), e2020GL087921. https://doi.org/10.1029/2020gl087921

Ganti, V., Straub, K. M., Foufoula-Georgiou, E., & Paola, C. (2011). Space-time dynamics of depositional systems: Experimental evidence and theoretical modeling of heavy-tailed statistics. *Journal of Geophysical Research*, *116*(F2), F02011. https://doi.org/10.1029/2010jf001893

Grimaud, J. L., Grall, C., Goodbred, S., Steckler, M. S., Sincavage, R., Pickering, J. L., et al. (2020). Flexural deformation controls on Late Quaternary sediment dispersal in the Garo-Rajmahal Gap, NW Bengal Basin. *Basin Research*, *32*(5), 1252–1270. https://doi.org/10.1111/bre.12425

Gross, L. J., & Small, M. J. (1998). River and floodplain process simulation for subsurface characterization. *Water Resources Research*, *34*(9), 2365–2376. https://doi.org/10.1029/98wr00777

Held, A. E. (2011). *Apport de la paléohydrologie dans la quantification des rôles respectifs du climat et de la tectonique des systèmes fluviatiles méandriformes fossiles: Application à des systèmes oligo-miocènes d'Europe occidentale*. ENMP.

Holbrook, J., & Miall, A. D. (2020). Time in the Rock: A field guide to interpreting past events and processes from a fragmentary siliciclastic archive. *Earth-Science Reviews*, *203*, 103121. https://doi.org/10.1016/j.earscirev.2020.103121

Howard, A. D. (1996). *Modeling channel evolution and floodplain morphology* (pp. 15–62).

Howard, A. H. (1992). Modeling channel migration and floodplain sedimentation in meandering streams. In *Lowland floodplain rivers. Geomorphological perspectives* (pp. 1–41). John Wiley.

Ikeda, S., Parker, G., & Sawai, K. (1981). Bend theory of river meanders. Part 1. Linear development. *Journal of Fluid Mechanics*, *112*, 363–377. https://doi.org/10.1017/s0022112081000451

Imran, J., Parker, G., & Pirmez, C. (1999). A nonlinear model of flow in meandering submarine and subaerial channels. *Journal of Fluid Mechanics*, *400*, 295–331. https://doi.org/10.1017/s0022112099006515

Jerolmack, D. J., & Mohrig, D. (2007). Conditions for branching in depositional rivers. *Geology*, *35*(5), 463–466. https://doi.org/10.1130/g23308a.1

Jerolmack, D. J., & Paola, C. (2010). Shredding of environmental signals by sediment transport. *Geophysical Research Letters*, *37*(19), L19401. https://doi.org/10.1029/2010gl044638

Jerolmack, D. J., & Sadler, P. (2007). Transience and persistence in the depositional record of continental margins. *Journal of Geophysical Research*, *112*(F3), F03S13. https://doi.org/10.1029/2006jf000555

Jobe, Z. R., Howes, N. C., Straub, K. M., Cai, D., Deng, H., Laugier, F. J., et al. (2020). Comparing aggradation, superelevation, and avulsion frequency of submarine and fluvial channels. *Frontiers of Earth Science*, *8*, 53. https://doi.org/10.3389/feart.2020.00053

Johannesson, H., & Parker, G. (1989). Velocity redistribution in meandering rivers. *Journal of Hydraulic Engineering*, *115*(8), 1019–1039. https://doi.org/10.1061/(asce)0733-9429(1989)115:8(1019)

Kim, W., Sheets, B. A., & Paola, C. (2010). Steering of experimental channels by lateral basin tilting. *Basin Research*, *22*(3), 286–301. https://doi.org/10.1111/j.1365-2117.2009.00419.x

Lemay, M. (2018). *Transposition à l'environnement turbiditique chenalisé d'un modèle de systèmes fluviatiles méandriformes pour la modélisation de réservoirs* (p. 145). Paris Sciences et Lettres.

Lemay, M., Grimaud, J.-L., Cojan, I., Rivoirard, J., & Ors, F. (2020). Geomorphic variability of submarine channelized systems along continental margins: Comparison with fluvial meandering channels. *Marine and Petroleum Geology*, *115*, 104295. https://doi.org/10.1016/j.marpetgeo.2020.104295

Leopold, L. B., & Wolman, M. G. (1960). River meanders. *GSA Bulletin*, *71*(6), 769–793. https://doi.org/10.1130/0016-7606(1960)71[769:rm]2.0.co;2

Limaye, A. B. S., & Lamb, M. P. (2013). A vector-based method for bank-material tracking in coupled models of meandering and landscape evolution. *Journal of Geophysical Research: Earth Surface*, *118*(4), 2421–2437. https://doi.org/10.1002/2013jf002854

Lopez, S. (2003). *Modélisation de réservoirs chenalisés méandriformes: Une approche génétique et stochastique*.

Lopez, S., Cojan, I., Rivoirard, J., & Galli, A. (2009). Process-based stochastic modelling: Meandering channelized reservoirs. In *Analogue and numerical Modelling of sedimentary systems: From Understanding to prediction* (pp. 139–144). Wiley.

Métivier, F., Gaudemer, Y., Tapponnier, P., & Klein, M. (1999). Mass accumulation rates in Asia during the Cenozoic. *Geophysical Journal International*, *137*(2), 280–318. https://doi.org/10.1046/j.1365-246x.1999.00802.x

Miall, A. D. (2015). Updating uniformitarianism: Stratigraphy as just a set of 'frozen accidents. *Geological Society, London, Special Publications*, *404*(1), 11–36. https://doi.org/10.1144/sp404.4

Mohrig, D., Heller, P. L., Paola, C., & Lyons, W. J. (2000). Interpreting avulsion process from ancient alluvial sequences: Guadalope-Matarranya system (northern Spain) and Wasatch Formation (western Colorado). *The Geological Society of America Bulletin*, *112*(12), 1787–1803. https://doi.org/10.1130/0016-7606(2000)112<1787:iapfaa>2.0.co;2

Morozova, G. S., & Smith, N. D. (2000). Holocene avulsion styles and sedimentation patterns of the Saskatchewan River, Cumberland Marshes, Canada. *Sedimentary Geology*, *130*(1–2), 81–105. https://doi.org/10.1016/s0037-0738(99)00106-2

Paola, C., Ganti, V., Mohrig, D., Runkel, A. C., & Straub, K. M. (2018). Time not our time: Physical controls on the preservation and measurement of geologic time. *Annual Review of Earth and Planetary Sciences*, *46*(1), 409–438. https://doi.org/10.1146/annurev-earth-082517-010129

Parker, G., Shimizu, Y., Wilkerson, G. V., Eke, E. C., Abad, J. D., Lauer, J. W., et al. (2011). A new framework for modeling the migration of meandering rivers. *Earth Surface Processes and Landforms*, *36*(1), 70–86. https://doi.org/10.1002/esp.2113

Pelletier, J. D., & Turcotte, D. L. (1997). Synthetic stratigraphy with a stochastic diffusion model of fluvial sedimentation. *Journal of Sedimentary Research*, *67*(6), 1060–1067.

Pizzuto, J. E. (1987). Sediment diffusion during overbank flows. *Sedimentology*, *34*(2), 301–317. https://doi.org/10.1111/j.1365-3091.1987.tb00779.x

Plotnick, R. E. (1986). A fractal model for the distribution of stratigraphic hiatuses. *The Journal of Geology*, *94*(6), 885–890. https://doi.org/10.1086/629094

Reesink, A., Van den Berg, J., Parsons, D. R., Amsler, M. L., Best, J. L., Hardy, R. J., et al. (2015). Extremes in dune preservation: Controls on the completeness of fluvial deposits. *Earth-Science Reviews*, *150*, 652–665. https://doi.org/10.1016/j.earscirev.2015.09.008

Retallack, G. (1984). Completeness of the rock and fossil record: Some estimates using fossil soils. *Paleobiology*, *10*(1), 59–78. https://doi.org/10.1017/s0094837300008022

Richards, K. S. (1982). *Rivers: Form and process in alluvial channels*. Methuen.

Sadler, P. M. (1981). Sediment accumulation rates and the completeness of stratigraphic sections. *The Journal of Geology*, *89*(5), 569–584. https://doi.org/10.1086/628623

Sadler, P. M., & Jerolmack, D. J. (2015). Scaling laws for aggradation, denudation and progradation rates: The case for time-scale invariance at sediment sources and sinks. *Geological Society, London, Special Publications*, *404*(1), 69–88. https://doi.org/10.1144/sp404.7

Sadler, P. M., & Strauss, D. J. (1990). Estimation of completeness of stratigraphical sections using empirical data and theoretical models. *Journal of the Geological Society*, *147*(3), 471–485. https://doi.org/10.1144/gsjgs.147.3.0471

Sahoo, H., Gani, M. R., Gani, N. D., Hampson, G. J., Howell, J. A., Storms, J. E. A., et al. (2020). Predictable patterns in stacking and distribution of channelized fluvial sand bodies linked to channel mobility and avulsion processes. *Geology*, *48*(9), 903–907. https://doi.org/10.1130/g47236.1

Scheidt, C., Fernandes, A. M., Paola, C., & Caers, J. (2016). Quantifying natural delta variability using a multiple-point geostatistics prior uncertainty model. *Journal of Geophysical Research: Earth Surface*, *121*(10), 1800–1818. https://doi.org/10.1002/2016jf003922

Schumer, R., Jerolmack, D., & McElroy, B. (2011). The stratigraphic filter and bias in measurement of geologic rates. *Geophysical Research Letters*, *38*(11), L11405. https://doi.org/10.1029/2011gl047118

Schumer, R., & Jerolmack, D. J. (2009). Real and apparent changes in sediment deposition rates through time. *Journal of Geophysical Research*, *114*(F3), F00A06. https://doi.org/10.1029/2009jf001266

Seminara, G. (2006). Meanders. *Journal of Fluid Mechanics*, *554*, 271–297. https://doi.org/10.1017/s0022112006008925

Straub, K. M., Duller, R. A., Foreman, B. Z., & Hajek, E. A. (2020). Buffered, incomplete, and shredded: The challenges of reading an imperfect stratigraphic record. *Journal of Geophysical Research: Earth Surface*, *125*(3), e2019JF005079. https://doi.org/10.1029/2019jf005079

Straub, K. M., & Esposito, C. R. (2013). Influence of water and sediment supply on the stratigraphic record of alluvial fans and deltas: Process controls on stratigraphic completeness. *Journal of Geophysical Research: Earth Surface*, *118*(2), 625–637. https://doi.org/10.1002/jgrf.20061

Straub, K. M., & Foreman, B. Z. (2018). Geomorphic stasis and spatiotemporal scales of stratigraphic completeness. *Geology*, *46*(4), 311–314. https://doi.org/10.1130/g40045.1

Straub, K. M., Paola, C., Mohrig, D., Wolinsky, M. A., & George, T. (2009). Compensational stacking of channelized sedimentary deposits. *Journal of Sedimentary Research*, *79*(9), 673–688. https://doi.org/10.2110/jsr.2009.070

Sun, T., Meakin, P., Jøssang, T., & Schwarz, K. (1996). A simulation model for meandering rivers. *Water Resources Research*, *32*(9), 2937–2954. https://doi.org/10.1029/96wr00998

Szewczyk, L., Grimaud, J. L., & Cojan, I. (2020). Experimental evidence for bifurcation angles control on abandoned channel fill geometry. *Earth Surface Dynamics*, *8*(2), 275–288. https://doi.org/10.5194/esurf-8-275-2020

Szewczyk, L., Grimaud, J.-L., Cojan, I., & Piégay, H. (2022). Bedload infilling and depositional patterns in chute cutoffs channels of a gravel-bed river: The Ain River, France. *Earth Surface Processes and Landforms*, *47*(2), 459–476. https://doi.org/10.1002/esp.5260

Tipper, J. C. (1998). The influence of field sampling area on estimates of stratigraphic completeness. *The Journal of Geology*, *106*(6), 727–740. https://doi.org/10.1086/516056

Tipper, J. C. (2015). The importance of doing nothing: Stasis in sedimentation systems and its stratigraphic effects. *Geological Society, London, Special Publications*, *404*(1), 105–122. https://doi.org/10.1144/sp404.6

Trampush, S., Hajek, E., Straub, K., & Chamberlin, E. (2017). Identifying autogenic sedimentation in fluvial-deltaic stratigraphy: Evaluating the effect of outcrop-quality data on the compensation statistic. *Journal of Geophysical Research: Earth Surface*, *122*(1), 91–113. https://doi.org/10.1002/2016jf004067

Trampush, S. M., & Hajek, E. A. (2017). Preserving proxy records in dynamic landscapes: Modeling and examples from the Paleocene-Eocene Thermal Maximum. *Geology*, *45*(11), 967–970. https://doi.org/10.1130/g39367.1

Wang, Y., Storms, J. E., Martinius, A. W., Karssenberg, D., & Abels, H. A. (2021). Evaluating alluvial stratigraphic response to cyclic and non-cyclic upstream forcing through process-based alluvial architecture modelling. *Basin Research*, *33*(1), 48–65. https://doi.org/10.1111/bre.12454

Weissmann, G., Hartley, A. J., Scuderi, L., Nichols, G., Owen, A., Wright, S., et al. (2015). Fluvial geomorphic elements in modern sedimentary basins and their potential preservation in the rock record: A review. *Geomorphology*, *250*, 187–219. https://doi.org/10.1016/j.geomorph.2015.09.005

Wheeler, H. E. (1958). Time-stratigraphy. *AAPG Bulletin*, *42*(5), 1047–1063. https://doi.org/10.1306/0BDA5AF2-16BD-11D7-8645000102C1865D

Williams, G. P. (1984). Paleohydrologic equations for rivers. In F. P. J., Costa (ed.), *Developments and applications of geomorphology*. Springer.

Williams, G. P. (1986). River meanders and channel size. *Journal of Hydrology*, *88*(1), 147–164. https://doi.org/10.1016/0022-1694(86)90202-7

Yan, N., Colombera, L., & Mountney, N. P. (2021). Evaluation of morphodynamic controls on the preservation of fluvial meander-belt deposits. *Geophysical Research Letters*, *48*(16), e2021GL094622. https://doi.org/10.1029/2021gl094622